Asymmetric Junctions in Metallic–Semiconducting–Metallic Heterophase MoS_2

Dipankar Saha, *Student Member, IEEE*, and Santanu Mahapatra, *Senior Member, IEEE*

***Abstract*— Symmetry of the source–channel and drain–channel junction is a unique property of a metal-oxide-semiconductor field effect transistor (MOSFET), which needs to be preserved while realizing sub-decananometer channel length devices using advanced technology. Employing experimental-findings-driven atomistic modeling techniques, we demonstrate that such symmetry might not be preserved in an atomically thin phase-engineered MoS_2-based MOSFET. It originates from the two distinct atomic patterns at phase boundaries (β and β^*) when the semiconducting phase (channel) is sandwiched between the two metallic phases (source and drain). We develop a geometrically optimized atomic model of two independent heterophase structures comprising β and β^* interfaces and study their electrical characteristics using density functional theory-nonequilibriumGreen's function formalism. We further study the effect of semiconductor doping on the transmission of those planar devices and show that irrespective of the doping concentration, these heterophase structures exhibit asymmetric barrier heights. Our findings could be useful for designing integrated circuits using such advanced transistors.**

***Index Terms*— Atomistic model, density functional theory (DFT)-nonequilibrium Green's function (NEGF) formalism, effective electron barrier, phase boundary, phase-engineered MoS_2.**

I. Introduction

NEW functionality of an electron device lays in the electrical characteristics of the interface formed between two dissimilar materials. With the advances in two-dimensional (2-D) materials, it is now possible to create atomically sharp in-plane or, out-of-plane interfaces by parallel stitching or stacking dissimilar atomic layers [1]–[6]. At this ultimate limit, where interface itself acts as a device [7], novel electronics and optoelectronics properties can be harnessed by selecting appropriate materials from the plethora of new 2-D materials [8], [9]. Understanding carrier transport at atomic scale is therefore an urgent need for these atomically thin heterojunctions.

New type of heterojunctions utilizing the lateral variation in number of layers has already been reported for epitaxial graphene and transition metal dichalcogenides (TMDs) [10], [11]. Giannazzo *et al.* [10] demonstrated the electronic transport and localized resistance enhancement across the junction of monolayer (1L)/bilayer (2L) epitaxial graphene on SiC. We find similar 1L/2L lateral heterojunctions, realized using ultrathin TMDs, e.g., $MoSe_2$ and WSe_2, as reported by Zhang *et al.* in [11]. Furthermore, they emphasized on the type-I band alignments (with well-defined interface states) of the 1L/2L atomically sharp line interfaces [11].

Apart from that, the recent demonstration of the coexistence of metallic and semiconducting phases on the same monolayer MoS_2 flake and its application in low resistive metal-MoS_2 contact have attracted tremendous attention [12]–[14]. In such phase-engineered monolayer MoS_2, the in-plane junctions are formed at phase boundaries and electrical properties of such interfaces could be assessed by atomistic modeling techniques [15]. It is worth noting that symmetric junctions at the source–channel and the drain–channel interfaces are expected for any good designed MOSFET for proper operation of several electronic circuits [16]. However, analyzing the annular dark field (ADF)-scanning transmission electron microscope (STEM) images of hetrophase MoS_2 crystals, two distinguishable phase boundaries are observed when the semiconducting phase (channel) is sandwiched between the two metallic phases (source/drain) [14]. Such observation motivates us to investigate if different atomic arrangements at phase boundaries could result in asymmetric junctions in an in-plane metallic–semiconducting–metallic (M-S-M) structure.

In this paper, we develop the geometrically optimized atomistic model for the M-S-M heterophase MoS_2 structure and reproduce the asymmetric atomic patterns at phase boundaries as observed in experimental ADF-STEM images. To probe further the electrical properties of the junctions, we conduct a first principles-based density functional theory (DFT)-nonequilibrium Green's function (NEGF) study on two independent device structures comprised of β and β^* phase boundaries. As electronic dopants are integral part of material design and play crucial role in adjusting the performance of an electronic device, we also investigate the effect of semiconductor doping on the effective barriers formed at

Manuscript received December 2, 2016; revised January 30, 2017, February 27, 2017, and March 5, 2017; accepted March 7, 2017. Date of publication March 27, 2017; date of current version April 19, 2017. This work was supported by the Science and Engineering Research Board, Department of Science and Technology, Government of India, under Grant SB/S3/EECE/0209/2015. The review of this brief was arranged by Editor M. M. Cahay.

The authors are with the Nano-Scale Device Research Laboratory, Department of Electronic Systems Engineering, Indian Institute of Science, Bengaluru 60012, India (e-mail: dipsah_etc@yahoo.co.in; santanu@dese.iisc.ernet.in).

Color versions of one or more of the figures in this paper are available online at http://ieeexplore.ieee.org.

Digital Object Identifier 10.1109/TED.2017.2680453

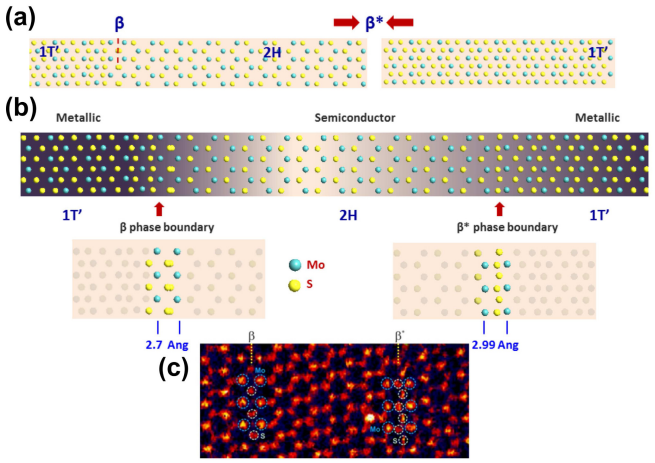

Fig. 1. (a) Alignment of the supercells to form β^* phase boundary. (b) Atomistic model of the M-S-M heterophase structure, having both β and β^* phase boundaries. (c) Adapted ADF image: [14, Fig. 4(c)] is rotated 180° and processed with standard software. Reused with permission from the authors.

junctions. By analyzing the zero bias transmission spectra and the energy-position resolved local density of states (LDOS) plots, we show that irrespective of the doping concentration, there is always a significant difference (∼0.2 V) in the effective electron barrier heights at two interfaces.

II. Methodology, Results, and Discussion

The DFT calculations are conducted using the Atomistix Tool Kit [17]. Here, we adopt the generalized gradient approximation as the exchange correlation along with the Perdew-Burke-Ernzerhof functional [18]. As the norm-conserving pseudopotentials, we use the OPENMX (Open source package for Material eXplorer) code [19]. Besides, the basis set for "Mo" and "S" atoms are taken as s3p2d1 and s2p2d1, respectively. In order to optimize the M-S-M planar heterophase structure, we use the limited-memory Broyden–Fletcher-Goldfarb–Shanno (LBFGS) algorithm (with force limit on each atom smaller than ∼0.08 eV/Å and maximum stress tolerance ∼0.001 eV/Å^3).

In Fig. 1, we present the details of the atomistic model, which is conceived using the 2H (semiconducting) and 1T′ (metallic) phases of monolayer MoS_2. As explained in [15], compared with the 1T polytype, its distorted counterpart, i.e., 1T′ is thermodynamically more stable [20], [21]. Also the absence of negative frequencies in the phonon bandstructure manifests the dynamical stability of 1T′ phase [15], [21]. To develop the atomistic model of the M-S-M structure, we use the 1T′-2H (having the β phase boundary) model of [15], and interface it with another 1T′ flake [aligning the supercells as shown in Fig. 1(a)] to form the distinct β^* phase boundary. The composite structure with both β and β^* phase boundaries can be seen in Fig. 1(b) (where, we have further highlighted the interfacing regions and their atomic patterns).

We find that the "Mo"-"Mo" distance for the β^* phase boundary is notably larger (2.99 Å) than that of the β one. We also notice that the nonoverlapping "S" atoms (along the thickness) of the β^* phase boundary, form a " S"-chain [in-plane view of Fig. 1(b)], which is not present in the case

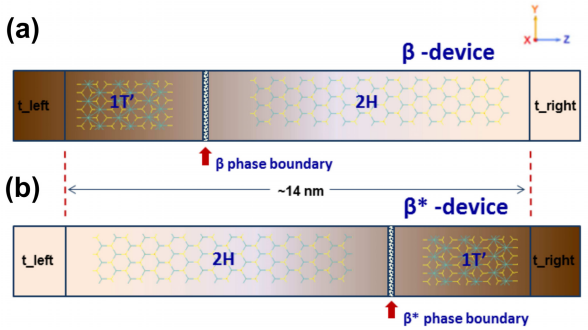

Fig. 2. The two-port devices: (a) β-device and (b) β^*-device.

of β interface. To validate the proposed atomic mode, we compare it with the ADF image [14, Fig. 4(c)] and observe good agreement. Though, Lin *et al.* [14] did not precisely differentiate between the two β interfaces, but considering the distinguishably different atomic arrangements [as shown in Fig. 1(c)], we call those interfacing regions as β and β^* phase boundaries. It should also be noted that, the study of [15] delineates the Schottky barrier nature of the two distinct types of phase boundaries, formed at the 2H-1T′ interfaces. However, it does not emphasize on the details of the M-S-M type heterophase structures. As mentioned earlier, to design atomically thin transistor channels, we need such M-S-M patterns induced locally in a single plane. Thereby, the atomic pattern in β^*, which is different from the γ [14], [15] one, requires additional investigation.

Fig. 2 shows the schematic diagrams of the two-port β-device and β^*-device, where the length and the width of the channels, are ∼140 Å and ∼9.58 Å, respectively. A vacuum region of ∼19 Å has been incorporated in the x-direction (i.e., perpendicular to the channel) to avoid any spurious interaction between periodic images [22]. Lengths of the left (t_left) and the right (t_right) electrodes are taken as 5.75 Å and 5.53 Å, respectively. It is important to note that, compared with the metallic (1T′) part, we have largely extended the semiconducting 2H region for effective screening of the potential drop across the interface. For the geometry optimization of those two independent devices (with β and β^* phase boundaries), we have utilized the aforementioned LBFGS algorithm. Moreover, for the electrical transport calculations (using DFT-NEGF formalism), we set the k-points in Monkhorst–Pack grid as $1 \times 9 \times 99$ (in the x-, y-, and z-directions, respectively) and the density mesh cutoff as 90 Hartree. For Poisson's equation, we use Dirichlet boundary condition along the transport direction (that is the z-direction), and periodic boundary conditions in the x- and y-directions. The lower bound of the contour integral is set as 3 Hartree.

In order to investigate the electrical nature of the asymmetric β^* phase boundary, we consider the two-port device structure of Fig. 2(b). For this device (with undoped semiconducting 2H region), we obtain the energy-position resolved LDOS diagram and the zero bias transmission spectrum as delineated in Fig. 3(a) and (b) respectively. Compared with the symmetric barrier (∼0.8 eV) of the β-device as reported in [15], we find that the barrier heights (for both types of charge carriers) are

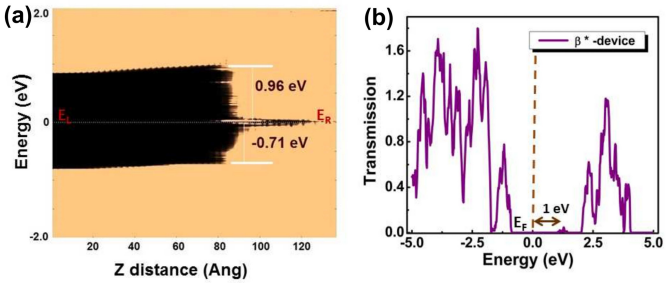

Fig. 3. (a) Energy-position-resolved LDOS diagram (with min. and max. values of device density of sates (1/eV) as 0 and 0.05, respectively), and (b) zero bias transmission spectrum of the β^* device.

not the same in the case of β^* device. Furthermore, for the device with β^*, the electron barrier is much larger ($\sim$0.96 eV) and the transmission states near the Fermi level (E_F) are heavily degraded. This ultimately leads to the reduced charge carrier conduction in β^*-devices.

To emphasize the rectifying characteristics of the individual heterophase structures, we dope the semiconducting part of the β-device and the β^*-device, with different doping densities. It is worth mentioning that the semiconducting 2H phase of MoS_2 is natively n-type-doped [23]. Some experimental studies further revealed that, due to imperfections and impurities, there might be large variation in the conductivity characteristics, across a small area of MoS_2 sheet [24], [25]. However, for device applications, in order to tune the electrical performance, a controllable doping strategy is essential. Suh *et al.* [23] proposed a method of substitutional Nb (niobium) doping, to attain stable p-type MoS_2. Nevertheless, a wide-range (taking both degenerate and nondegenerate regimes into account) controllable n-type doping for MoS_2 on the phosphorus silicate glass (PSG) substrate has been demonstrated in [26]. This is achieved via process steps [26], e.g., thermal activation, optical activation, adjustment of the concentration of P atoms in PSG, and so on.

However, here in this brief, we have only emphasized on the n-type doping of MoS_2, and effectively doped the semiconducting regions by incorporating n-type compensation-charge [27], [28]. Such an effective doping scheme is really advantageous, since it does not depend on the exact details of the dopant atoms [28]. Taking moderate and high doping densities into consideration (3.4×10^{17} /cm^3 and 1×10^{19} /cm^3), we set the values of "atomic compensation charge" β-device and β^*-device [29]. Hereafter, devices with moderate and high doping will be called as device1 and device2, respectively. Fig. 4(a) and (b) shows the energy-position-resolved LDOS diagrams of β-device1 and β-device2, respectively. At equilibrium, considering the β-device1 where the 2H side is moderately doped into n-type, we find a significant reduction in the effective electron barrier. Moreover, with increase of doping density, this barrier gets further lowered in the case of β-device2, making the tunneling phenomenon to play its role in charge carrier transport calculation [30]. Similar effects of semiconductor doping can be observed for the β^*-devices [Fig. 4(c) and (d)]. We also find that high doping concentration significantly improves the poor screening along the semiconducting (2H) part.

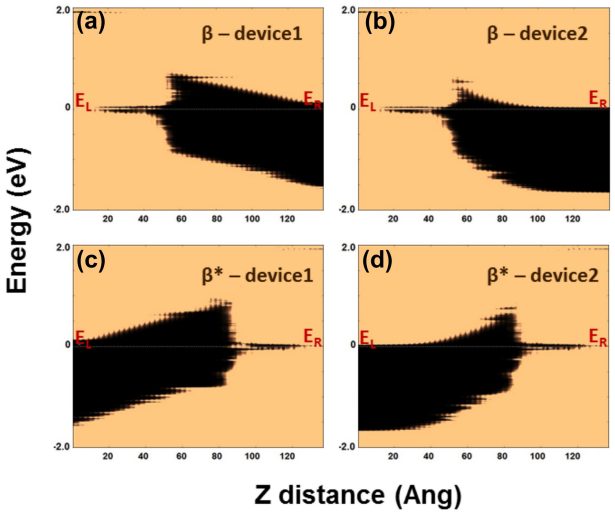

Fig. 4. LDOS diagrams obtained for the β-devices and the β^*-devices, considering moderate and high doping densities.

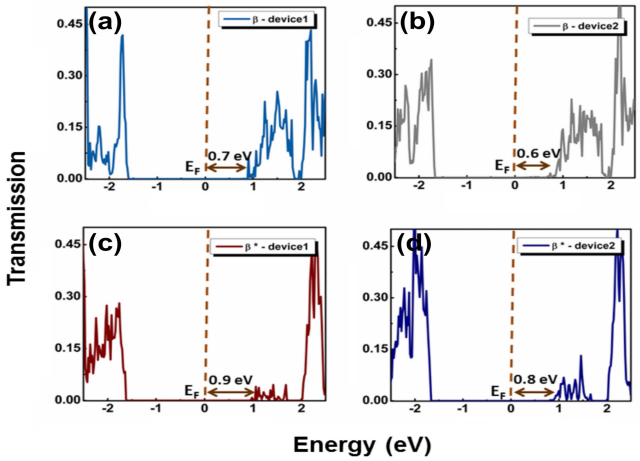

Fig. 5. Transmission spectra of the β-devices ((a), and (b)) and the β^*-devices ((c), and (d)), considering moderate and high doping densities.

Next, we delve into a quantitative analysis by comparing the zero bias transmission spectra (upspin components) of Fig. 5. Forbidden region between the E_F and the transmission states corresponding to the effective conduction band edge is $\sim$0.7 eV for the β-device1 [Fig. 5(a)]. As we further increase the doping density for β-device2, the conduction band edge shifts much closer to the E_F [$\sim$0.6 eV, shown in Fig. 5(b)]. However, for the β^*-devices, we observe significant degradation in the transmission states within the range of 0–2 eV [Fig. 5(c), (d)], making the devices less conducive to the charge carrier transport. This actually arises from the electrical nature of the scattering region formed with β^* phase boundary. Besides, the larger ($\sim$1 eV) effective electron barrier of the undoped β^* device [Fig. 3(a)] gets reduced to $\sim$0.9 eV (β^*-device1) and $\sim$0.8 eV (β^*-device2), as the result of moderate and high n-type doping. It is interesting to note that the increase in semiconductor doping (from a moderate to a high value) necessarily lowers the threshold of the β and β^*-devices, by a certain amount. Nevertheless, this could be crucial in achieving higher ON-current values at relatively lower bias voltages.

III. Conclusion

We conceive atomic models to delineate the asymmetry in boundaries when a semiconducting phase of MoS_2 is sandwiched between the two metallic phases. Using first principles-based quantum transport formalism, we show that irrespective of doping concentration, a difference of 0.2 V in effective electron barrier height is observed between two interfaces.

Acknowledgment

The authors would like to thank Dr. Y.-C. Lin and Dr. K. Suenaga of AIST, Japan, for the valuable discussions. They would also like to thank G.-N. Kadloor, DESE-IISc, for processing the adapted ADF image.

References

[1] Y. Gong *et al.*, "Vertical and in-plane heterostructures from WS_2/MoS_2 monolayers," *Nature Mater.*, vol. 13, pp. 1135–1142, Dec. 2014, doi: 10.1038/NMAT4091.

[2] R. Cheng *et al.*, "Electroluminescence and photocurrent generation from atomically sharp WSe_2/MoS_2 heterojunction $p-n$ diodes," *Nano Lett.*, vol. 14, pp. 5590–5597, Aug. 2014, doi: 10.1021/nl502075n.

[3] X. Ling *et al.*, "Parallel stitching of 2D materials," *Adv. Mater.*, vol. 28, no. 12, pp. 2322–2329, 2016, doi: 10.1002/adma.201505070.

[4] F. W. Chen, H. Ilatikhameneh, T. A. Ameen, G. Klimeck, and R. Rahman, "Thickness engineered tunnel field-effect transistors based on phosphorene," *IEEE Electron Device Lett.*, vol. 38, no. 1, pp. 130–133, Jan. 2017, doi: 10.1109/LED.2016.2627538.

[5] A. Szabo, S. J. Koester, and M. Luisier, "Metal-dichalcogenide hetero-TFETs: Are they a viable option for low power electronics?" in *Proc. 72nd Device Res. Conf.*, Santa Barbara, CA, USA, 2014, pp. 19–20.

[6] F. Chen, H. Ilatikhameneh, Y. Tan, D. Valencia, G. Klimeck, and R. Rahman. (Sep. 2016). "Transport in vertically stacked heterostructures from 2D materials." [Online]. Available: https://arxiv.org/abs/1608.05057

[7] A. Pant *et al.*, "Fundamentals of lateral and vertical heterojunctions of atomically thin materials," *Nanoscale*, vol. 8, no. 7, pp. 3870–3887, 2016.

[8] F. W. Chen, H. Ilatikhameneh, G. Klimeck, Z. Chen, and R. Rahman, "Configurable electrostatically doped high performance bilayer graphene tunnel FET," *IEEE J. Electron Devices Soc.*, vol. 4, no. 3, pp. 124–128, May 2016, doi: 10.1109/JEDS.2016.2539919.

[9] H. Ilatikhameneh, T. Ameen, B. Novakovic, Y. Tan, G. Klimeck, and R. Rahman, "Saving Moore's law down to 1 nm channels with anisotropic effective mass," *Sci. Rep.*, vol. 6, Aug. 2016, Art. no. 31501, doi: 10.1038/srep31501.

[10] F. Giannazzo, I. Deretzis, A. La Magna, F. Roccaforte, and R. Yakimova, "Electronic transport at monolayer-bilayer junctions in epitaxial graphene on SiC," *Phys. Rev. B, Condens. Matter*, vol. 86, p. 235422, Dec. 2012.

[11] C. Zhang *et al.*, "Visualizing band offsets and edge states in bilayer-monolayer transition metal dichalcogenides lateral heterojunction," *Nature Commun.*, vol. 7, Jan. 2016, Art. no. 10349, doi: 10.1038/ncomms10349.

[12] G. Eda, T. Fujita, H. Yamaguchi, D. Voiry, M. Chen, and M. Chhowalla, "Coherent atomic and electronic heterostructures of single-layer MoS_2," *ACS Nano*, vol. 6, no. 8, pp. 7311–7317, Jul. 2012.

[13] R. Kappera *et al.*, "Phase-engineered low-resistance contacts for ultrathin MoS_2 transistors," *Nature Mater.*, vol. 13, pp. 1128–1134, Sep. 2014, doi: 10.1038/nmat4080.

[14] Y.-C. Lin, D. O. Dumcenco, Y.-S. Huang, and K. Suenaga, "Atomic mechanism of the semiconducting-to-metallic phase transition in single-layered MoS_2," *Nature Nanotechnol.*, vol. 9, pp. 391–396, Apr. 2014.

[15] D. Saha and S. Mahapatra, "Atomistic modeling of the metallic-to-semiconducting phase boundaries in monolayer MoS_2," *Appl. Phys. Lett.*, vol. 108, p. 253106, Jun. 2016. [Online]. Available: http://dx.doi.org/10.1063/1.4954257.

[16] C. C. McAndrew, "Validation of MOSFET model source-drain symmetry," *IEEE Trans. Electron Devices*, vol. 53, no. 9, pp. 2202–2206, Sep. 2006, doi: 10.1109/TED.2006.881005.

[17] NanoLab. *QuantumWise Atomistix ToolKit (ATK) with Virtual NanoLab. Version 2015.1*, accessed on Mar. 5, 2017. [Online]. Available: http://quantumwise.com/

[18] J. P. Perdew, K. Burke, and M. Ernzerhof, "Generalized gradient approximation made simple," *Phys. Rev. Lett.*, vol. 77, no. 18, pp. 3865–3868, Oct. 1996. [Online]. Available: https://doi.org/10.1103/PhysRevLett.77.3865.

[19] T. Ozaki and H. Kino, "Numerical atomic basis orbitals from H to KR," *Phys. Rev. B, Condens. Matter*, vol. 69, p. 195113, May 2004, doi: 10.1103/PhysRevB.69.195113.OMX_2.

[20] G. Gao, Y. Jiao, F. Ma, Y. Jiao, E. Waclawik, and A. Du, "Charge mediated semiconducting-to-metallic phase transition in molybdenum disulfide monolayer and hydrogen evolution reaction in new 1T' phase," *J. Phys. Chem. C*, vol. 119, pp. 13124–13128, May 2015.

[21] X. Qian, J. Liu, L. Fu, and J. Li, "Quantum spin Hall effect in two-dimensional transition metal dichalcogenides," *Science*, vol. 346, no. 6215, pp. 1344–1347, Dec. 2014, doi: 10.1126/science.1256815.

[22] D. Saha and S. Mahapatra, "Theoretical insights on the electrothermal transport properties of monolayer MoS_2 with line defects," *J. Appl. Phys.*, vol. 119, p. 134304, Apr. 2016. [Online]. Available: http://dx.doi.org/10.1063/1.4945582.

[23] J. Suh *et al.*, "Doping against the native propensity of MoS_2: Degenerate hole doping by cation substitution," *Nano Lett.*, vol. 14, no. 12, pp. 6976–6982, 2014.

[24] S. McDonnell, R. Addou, C. Buie, R. M. Wallace, and C. L. Hinkle, "Defect-dominated doping and contact resistance in MoS_2," *ACS Nano*, vol. 8, no. 3, pp. 2880–2888, Jan. 2014.

[25] R. Addou *et al.*, "Impurities and electronic property variations of natural MoS_2 crystal surfaces," *ACS Nano*, vol. 9, no. 9, pp. 9124–9133, 2015.

[26] H.-Y. Park *et al.*, "Wide-range controllable n-doping of molybdenum disulfide (MoS_2) through thermal and optical activation," *ACS Nano*, vol. 9, no. 3, pp. 2368–2376, 2015.

[27] M. Brandbyge, J.-L. Mozos, P. Ordejón, J. Taylor, and K. Stokbro, "Density-functional method for nonequilibrium electron transport," *Phys. Rev. B, Condens. Matter*, vol. 65, p. 165401, Mar. 2002.

[28] D. Stradi, U. Martinez, A. Blom, M. Brandbyge, and K. Stokbro, "General atomistic approach for modeling metal-semiconductor interfaces using density functional theory and nonequilibrium Green's function," *Phys. Rev. B, Condens. Matter*, vol. 93, p. 155302, Apr. 2016, doi: 10.1103/PhysRevB.93.155302.

[29] Y. Zhang *et al.*, "Thickness considerations of two-dimensional layered semiconductors for transistor applications," *Sci. Rep.*, vol. 6, p. 29615, Jul. 2016, doi: 10.1038/srep29615.

[30] H. Ilatikhameneh, R. B. Salazar, G. Klimeck, R. Rahman, and J. Appenzeller, "From Fowler–Nordheim to nonequilibrium Green's function modeling of tunneling," *IEEE Trans. Electron Device*, vol. 63, no. 7, pp. 2871–2878, Jul. 2016, doi: 10.1109/TED.2016.2565582.

Dipankar Saha (S'12) received the M.Tech. degree from Jadavpur University, Kolkata, India, in 2013. He is currently pursuing the Ph.D. degree with the Nano Scale Device Research Laboratory, Department of Electronic Systems Engineering, Indian Institute of Science, Bangaluru 560012, India.

His current research interests include electrothermal transport in nanoelectronic devices and modeling and simulation of nano-scaled devices with 2-D channel materials.

Santanu Mahapatra (M'08–SM'10) received the Ph.D. degree from the Ecole Polytechnique Federale de Lausanne, Lausanne, Switzerland, in 2005.

He is currently a Professor with Indian Institute of Science , Bangaluru, India. His current research interests include atomistic, device, and compact modeling. Dr. Mahapatra was a recipient of the Ramanna Fellowship from the Department of Science and Technology, Government of India, for his contribution in compact modeling, in 2012.